INTERFACE

royalsocietypublishing.org/journal/rsif

Research

Cite this article: Doerries TJ, Chechkin AV, Metzler R. 2022 Apparent anomalous diffusion and non-Gaussian distributions in a simple mobile–immobile transport model with Poissonian switching. *J. R. Soc. Interface* **19**: 20220233.
https://doi.org/10.1098/rsif.2022.0233

Received: 22 March 2022
Accepted: 15 June 2022

Subject Category:
Life Sciences–Physics interface

Subject Areas:
biophysics, environmental science

Keywords:
diffusion, mobile–immobile model, tau proteins

Author for correspondence:
Ralf Metzler
e-mail: rmetzler@uni-potsdam.de

Apparent anomalous diffusion and non-Gaussian distributions in a simple mobile–immobile transport model with Poissonian switching

Timo J. Doerries[1], Aleksei V. Chechkin[1,2,3] and Ralf Metzler[1]

[1]Institute of Physics and Astronomy, University of Potsdam, 14476 Potsdam, Germany
[2]Faculty of Pure and Applied Mathematics, Hugo Steinhaus Center, Wrocław University of Science and Technology, Wyspianskiego 27, 50-370 Wrocław, Poland
[3]Akhiezer Institute for Theoretical Physics, National Science Center 'Kharkiv Institute of Physics and Technology', 61108 Kharkiv, Ukraine

RM, 0000-0002-6013-7020

We analyse mobile–immobile transport of particles that switch between the mobile and immobile phases with finite rates. Despite this seemingly simple assumption of Poissonian switching, we unveil a rich transport dynamics including significant transient anomalous diffusion and non-Gaussian displacement distributions. Our discussion is based on experimental parameters for tau proteins in neuronal cells, but the results obtained here are expected to be of relevance for a broad class of processes in complex systems. Specifically, we obtain that, when the mean binding time is significantly longer than the mean mobile time, transient anomalous diffusion is observed at short and intermediate time scales, with a strong dependence on the fraction of initially mobile and immobile particles. We unveil a Laplace distribution of particle displacements at relevant intermediate time scales. For any initial fraction of mobile particles, the respective mean squared displacement (MSD) displays a plateau. Moreover, we demonstrate a short-time cubic time dependence of the MSD for immobile tracers when initially all particles are immobile.

1. Introduction

Already in the 1960s, there was considerable interest in the transport of chemical tracers, especially pesticides, nitrates and heavy metals through water-carrying layers of soil [1]. A typical description for such contaminant transport was the diffusion–advection equation (sometimes called the convective–dispersive equation) [2]

$$\frac{\partial}{\partial t}C(x,t) = D\frac{\partial^2}{\partial x^2}C(x,t) - v\frac{\partial}{\partial x}C(x,t), \tag{1.1}$$

where $C(x, t)$ is the contaminant concentration at distance x after time t, v is an advection velocity chosen as zero in the following and D is the diffusion constant (dispersion coefficient typically measured in units of $\mathrm{cm}^2\,\mathrm{d}^{-1}$). Measurements revealed, however, that not all of the contaminant concentration was mobile at any given time, but that a fraction could be (transiently) trapped in stagnant volumes. Building on earlier models by Deans [3] and Coats & Smith [4], van Genuchten & Wierenga [5] analysed the exchange between mobile ($C_m(x, t)$) and immobile ($C_{im}(x, t)$) fractions. The mobile–immobile model under advection–diffusion conditions has been investigated intensively in the literature over the last 50 years [3,4,6–8]. Application of the mobile–immobile model includes the advective–diffusive transport of contaminants in the mobile domain of porous media [3,4,6–8], electrons in photoconductors [9], chemicals in chromatography [10] and adsorbing solutes in soil [11]. In many

THE ROYAL SOCIETY PUBLISHING

geophysical systems equations of the type (1.1) are modified to account for anomalous transport, in which molecular transport no longer follows the linear time dependence $\langle \Delta x^2(t) \rangle = \langle x^2(t) \rangle - \langle x(t) \rangle^2 = 2Dt$ of Brownian motion, but follows laws of the type $\langle \Delta x^2(t) \rangle = 2D_\alpha t^\alpha$, for which $\alpha \neq 1$ [12]. Indeed, such transport anomalies were found on large field experiments, up to kilometre scales [13,14]. In such systems, the mobile–immobile transport model is replaced by models in which generalized transport terms are incorporated [15,16]. This type of model, in contrast to equation (1.1), is characterized by non-Gaussian distributions [12].

Motivated by concrete biological examples, we here study a seemingly simple version of the mobile–immobile transport model, in which particles switch between a freely diffusive phase and an immobile, stagnant phase. Even for the Poissonian switching dynamics considered here between the mobile and immobile phases and for biologically relevant parameters, we demonstrate the existence of a significant, transient anomalous–diffusive regime with a distinct non-Gaussian displacement distribution.

In fact, various components of biological cells, including tau proteins, synaptic vesicles in hippocampal neurons, glucocorticord receptors, calcium-sensing proteins and transcription factors at the junction of the endoplasmic reticulum and the plasma membrane, undergo diffusion with transient immobilization [17–24]. Another example is given by the diffusion and target search of DNA-binding proteins along DNA molecules. For instance, the core domain of the tumour suppressor p53, the damage detection complex Rad4-Rad23 and the architectural DNA-binding protein Fis repeatedly attach to and detach from the DNA during the target search [25–29]. We here focus on tau proteins, which transiently bind to microtubules in axons of neuronal cells and are immobilized in the bound state, as schematically depicted in figure 1. Tau proteins stabilize microtubules that give structure to cells [30]. Alzheimer's disease is associated with tau proteins losing the ability to bind to microtubules [30,31]. This effectively destabilizes the microtubules and leads to neurodegeneration [30,31]. Owing to the extremely elongated shape of the axon, the motion of tau proteins can be effectively described in one dimension [17]. If the immobilization time follows an exponential distribution with mean $\tau_{\rm im}$ and tracers immobilize with rate $\tau_{\rm m}^{-1}$, i.e. a Poissonian dynamics, as assumed in [17], the motion can be described by the mobile–immobile model

$$\left.\begin{aligned} &\frac{\partial}{\partial t} n_{\rm m}(x,t) = -\frac{1}{\tau_{\rm m}} n_{\rm m}(x,t) + \frac{1}{\tau_{\rm im}} n_{\rm im}(x,t) + D\frac{\partial^2}{\partial x^2} n_{\rm m}(x,t) \\ \text{and } &\frac{\partial}{\partial t} n_{\rm im}(x,t) = -\frac{1}{\tau_{\rm im}} n_{\rm im}(x,t) + \frac{1}{\tau_{\rm m}} n_{\rm m}(x,t). \end{aligned}\right\} \tag{1.2}$$

Here, $n_{\rm m}(x,\ t)$ and $n_{\rm im}(x,\ t)$ denote the line densities of mobile and bound tau proteins, respectively, with physical dimension [1/length]. The diffusion coefficient of the mobile tracers is D. Since we are dealing with a system of non-interacting particles, we use a probabilistic formulation according to which the total concentration $n_{\rm tot}(x,\ t) = n_{\rm m}(x,\ t) + n_{\rm im}(x,\ t)$ is normalized to unity, $\int_{-\infty}^{\infty} n_{\rm tot}(x,\ t)dx = 1$. The line densities $n_{\rm m}(x,\ t)$ and $n_{\rm im}(x,\ t)$ are then the respective fractions. Equations (1.2) were analysed in three dimensions for an equilibrium fraction of initially mobile tracers, finding Fickian yet non-Gaussian diffusion [32]. Accordingly, the mean squared displacement (MSD) of the total concentration $n_{\rm tot}$ grows linearly at all times, and under certain conditions a non-Gaussian distribution emerges [32].

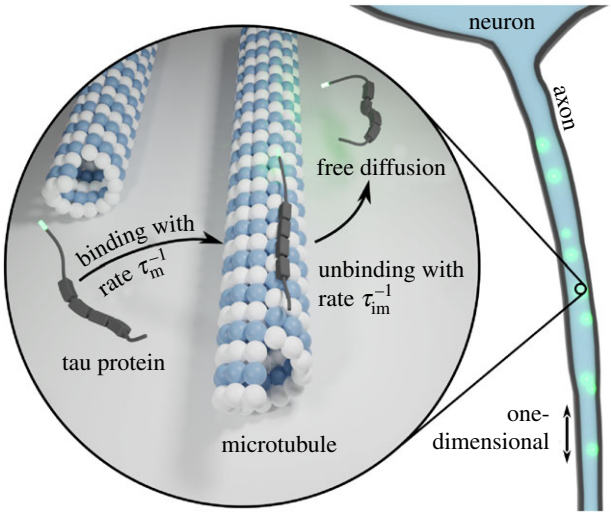

Figure 1. Schematic of tau protein dynamics in axons of neuronal cells. Diffusing tau proteins bind to longitudinally aligned microtubules inside the axon with the rate $\tau_{\rm m}^{-1}$. Upon binding, they remain immobile for the average duration $\tau_{\rm im}$ and unbind with the rate $\tau_{\rm im}^{-1}$. The green markers represent fluorescent proteins attached to the tau proteins. Because of the elongated shape of the axons, the tau protein dynamic can effectively be described in one dimension. In our model, we assume a homogeneous binding site density.

Such Fickian yet non-Gaussian diffusion has been shown to occur for the motion of colloidal beads on phospholipid bilayer tubes, molecules at surfaces and colloids in a dense matrix of micropillars, where the colloids can get trapped in pockets [33–35]. Fickian yet non-Gaussian diffusion with a finite correlation time beyond which the displacement probability density function (PDF) crosses over to a Gaussian with an effective diffusivity arises in diffusing–diffusivity models, in which the diffusivity of individual tracers varies stochastically over time [36–41]. Direct examples for such randomly evolving diffusion coefficients (mobilities) are indeed known from lipids in protein-crowded bilayer membranes [42], shape-shifting protein molecules [43] or (de)polymerizing oligomer chains [44,45]. In other systems, an intermittent plateau emerges in the MSD; for instance, for two-dimensional fluids confined in a random matrix of obstacles or a porous cavity, in which trapping in finite pockets plays a key role [46–48]. We also mention plateaus in the MSD of both two- and three-dimensional isotropic Lennard-Jones binary liquids [49]. In most of the systems mentioned here, the PDF crosses over from an exponential (Laplace) PDF to a Gaussian. In the following, we explicitly show how a Laplace distribution with fixed scale parameters arises at intermediate time scales in our mobile–immobile model, paired with transient anomalous diffusion.

In what follows, we consider three initial conditions: an equilibrium fraction of mobile tracers and a scenario in which initially all tracers are mobile or immobile. These experimentally feasible situations significantly change the diffusion at short and intermediate time scales, at which apparent anomalous diffusion arises with slow-down and plateau-like behaviour, or ballistic diffusion, respectively. Together with the transient non-Gaussian displacement PDF, this behaviour is remarkably rich, given the simplicity of the governing equation (1.2). We individually analyse the motion of the

mobile and immobile population of tracers, made possible by the formulation of separate densities for mobile and immobile particles in this modelling approach. One physical incentive to do so is that the function of the tau proteins depends on their binding state [30]. Only bound tau proteins stabilize microtubules, or transcription factors modulate gene expression when bound to the DNA [21,30]. In some situations, only the mobile or immobile tracers can be measured. An example is given by combining total internal reflection fluorescence microscopy with fluorescently labelled single-stranded DNA, which binds to the microscope coverslip [50].

We present general results for the mobile and immobile concentrations and the MSD for arbitrary fractions of initially mobile tracers in §2. Sections 3–5 present concrete results and detailed discussions for different fractions of initial mobile particle concentrations; respectively, we start with the cases when all tracers are initially mobile and immobile and commence with an equilibrium fraction of mobile tracers. We conclude in §6.

2. Model and general solutions

We consider the mobile–immobile model equations (1.2) for the initial conditions $n_m(x, 0) = f_m\delta(x)$ and $n_{im}(x, 0) = f_{im}\delta(x)$, where f_m and f_{im} denote the fractions of initially mobile and immobile tracers, respectively, with the normalization $f_m + f_{im} = 1$. This formulation is suitable for typical single-particle tracking experiments used in biological and soft matter systems. They are also relevant for geophysical experiments, in which point-like injection of tracers is used. In this section, we keep the fractions f_m and f_{im} arbitrary and choose specific values in the following three sections.

In what follows, we use the concrete parameters $D = 13.9$ $(\mu m)^2\,s^{-1}$, $\tau_m = 0.16$ s and $\tau_{im} = 7.7$ s from [17] in all figures and neglect the vanishingly small advection velocity $v = 0.002\,\mu m\,s^{-1}$.[1] The values were obtained from experiments using the fluorescent decay after the photoactivation technique [17]. Let us briefly address the experimental origin of the time-scale separation between τ_m and τ_{im}. From single-particle tracking experiments of single-stranded DNA or tau proteins, immobilization times during the particle motion can be extracted [18,50]. The experiments for the tau proteins in [18] provided two-dimensional information and revealed relatively short residence times of the tau proteins on the microtubules, when compared with mobile times [18]. By contrast, the fluorescence decay after photoactivation (FDAP) experiment in one dimension along the axon direction, here denoted as the x variable, revealed long residence times and short mobile periods: $\tau_{im} \approx 48\tau_m$ [17]. This seeming contradiction can be resolved when examining more closely the two-dimensional trajectories in the electronic supplementary material of [18]. Namely, the microtubules inside the axon are aligned in parallel with the axon axis, as also shown in figure 1. While a single binding event is short, an unbound particle quickly rebinds to a parallel, nearby microtubule after a short distance covered by diffusion perpendicular to the axon axis. This perpendicular motion does not contribute to the one-dimensional motion in the x-direction and thus, while individual binding times are relatively short, *effective* binding times appear much longer in the projection to one dimension. Since we are only interested in the one-dimensional motion, we use the parameters of [17] and hence long immobilization times.

2.1. Mobile and immobile concentration profiles

We consider the Fourier–Laplace transform of the concentrations and solve for $n_m(k, s)$, $n_{im}(k, s)$ and $n_{tot}(k, s)$ in expressions (A 1) and (A 2), in which the Fourier wavenumber k corresponds to the distance x in real space and the Laplace variable s is conjugated to time t; see appendix A for details. We denote functions in Fourier or Laplace space solely by replacing the explicit dependencies on the respective arguments. The relations in the Fourier–Laplace domain can be Fourier-inverted, and we obtain the expressions in the Laplace domain,

$$n_m(x, s) = \left(f_m + f_{im}\frac{1}{1+s\tau_{im}}\right)\frac{1}{\sqrt{4\phi(s)D}}\,e^{-\sqrt{\phi(s)/D}|x|}, \quad (2.1)$$

$$\begin{aligned} n_{im}(x, s) = {} & \left(f_m + f_{im}\frac{1}{1+s\tau_{im}}\right) \\ & \times \frac{\tau_{im}/\tau_m}{1+s\tau_{im}}\frac{1}{\sqrt{4\phi(s)D}}\,e^{-\sqrt{\phi(s)/D}|x|} \\ & + f_{im}\frac{\tau_{im}}{1+s\tau_{im}}\,\delta(x) \end{aligned} \quad (2.2)$$

and

$$\begin{aligned} n_{tot}(x, s) = {} & \frac{f_m + f_{im}\dfrac{1}{1+s\tau_{im}}}{s}\,\phi(s) \\ & \times \frac{1}{\sqrt{4\phi(s)D}}\,e^{-\sqrt{4\phi(s)/D}|x|} \\ & + f_{im}\frac{\tau_{im}}{1+s\tau_{im}}\,\delta(x), \end{aligned} \quad (2.3)$$

as functions of x and s with $\phi(s) = s[1 + \tau_{im}\tau_m^{-1}/(1 + s\tau_{im})]$. These expressions are valid for all s and hence for all times t. A numerical Laplace inversion then provides the densities for any specified time. Remarkably, it turns out that the density of mobile tracers, which were initially immobile, is proportional to the density of immobile tracers, which were initially mobile. This can be seen by setting $f_m = 0$ or $f_{im} = 0$ in (2.1) and (2.2), respectively. This proportionality holds for all s and hence at all times. We obtain the long-time Gaussian limit of the full concentration in B.3,

$$n_{tot}(x, t) \sim \frac{1}{\sqrt{4\pi D_{eff}t}}\exp\left(-\frac{x^2}{4D_{eff}t}\right), \quad t \gg \tau_m, \tau_{im}, \quad (2.4)$$

with $D_{eff} = D/(1 + \tau_{im}/\tau_m)$. Note that, for asymptotic equalities, we use the $\sim$ symbol. In fact, independent of the ratio f_m and f_{im} we asymptotically obtain a Gaussian distribution in which the diffusivity is reduced to the effective diffusivity D_{eff}. The mobile and immobile concentrations are asymptotically equivalent to (2.4) up to a scalar f_j^{eq} defined below [16].

2.2. Moments

In general, the fractions $\overline{n}_m$ and $\overline{n}_{im}$ of mobile and immobile tracers, initially fixed as f_m and f_{im}, change over time. To obtain the respective numbers, we integrate the tracer densities over space. This corresponds to setting $k = 0$ in the Fourier–Laplace transforms $n_m(k, s)$ and $n_{im}(k, s)$ of the densities. After Laplace inversion, we find

$$\overline{n}_m(t) = \frac{\tau_m}{\tau_m + \tau_{im}} + \frac{f_m\tau_{im} - f_{im}\tau_m}{\tau_m + \tau_{im}}\exp(-[\tau_m^{-1} + \tau_{im}^{-1}]t) \quad (2.5)$$

and

$$\overline{n}_{im}(t) = \frac{\tau_{im}}{\tau_m + \tau_{im}} - \frac{f_m\tau_{im} - f_{im}\tau_m}{\tau_m + \tau_{im}}\exp(-[\tau_m^{-1} + \tau_{im}^{-1}]t), \quad (2.6)$$

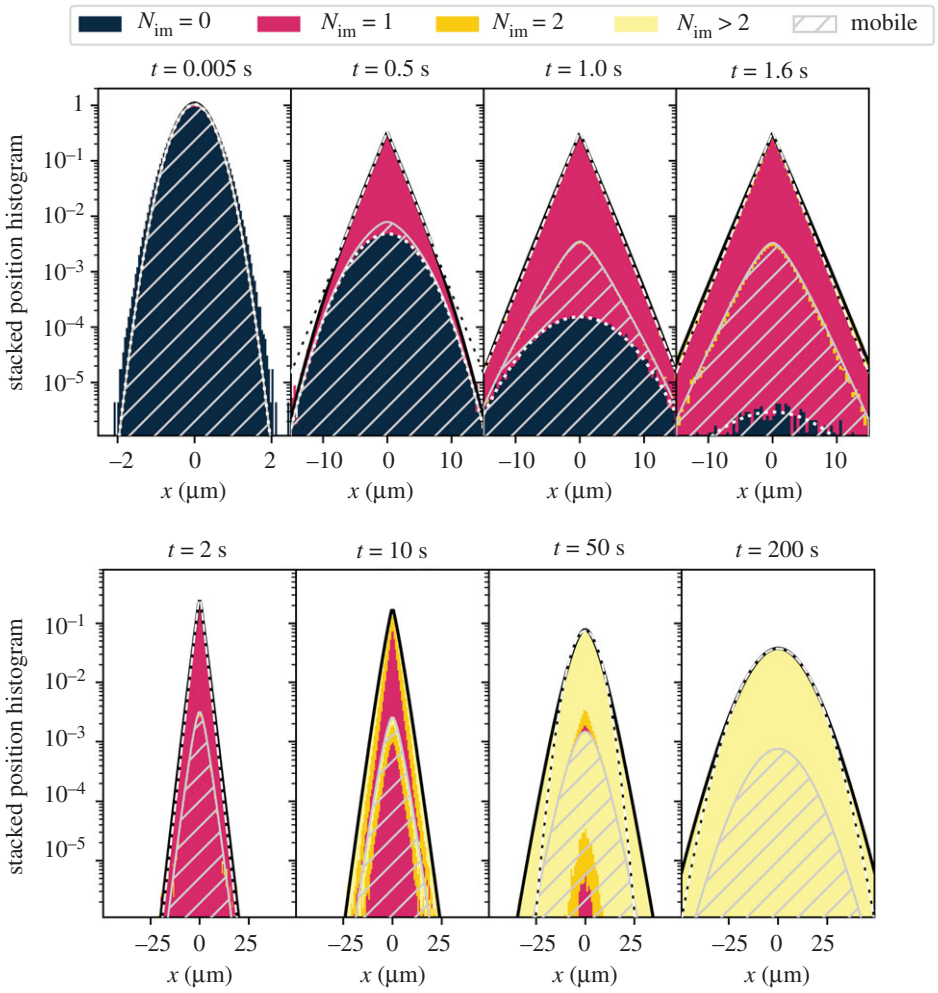

Figure 2. Concentration profiles for mobile initial conditions. The solid black line shows $n_{tot}(x, t)$ and the grey striped area $n_m(x, t)$, obtained via Laplace inversion of relations (2.1) and (2.3). Colours indicate the number of immobilization events of particles from a Brownian dynamics simulation with 5×10^6 trajectories in a stacked histogram. The striped area denotes mobile particles and the white dotted line denotes initially mobile tracers that have not yet been immobilized up to the indicated time t (3.2); this result almost coincides with the full concentration in the top left panel. For $t = 0.5$ s to 2 s, the white dashed line shows the Laplacian (3.5); for $t = 50$ s and 200 s, it shows the long-time Gaussian (2.4).

with $\overline{n}_m(t) + \overline{n}_{im}(t) = 1$. In the long-time limit $t \gg \tau_m, \tau_{im}$, the fractions of mobile and immobile tracers reach the stationary values $f_m^{eq} = \tau_m/(\tau_m + \tau_{im})$ and $f_{im}^{eq} = \tau_{im}/(\tau_m + \tau_{im})$, respectively. Our approach of splitting the total concentration into mobile and immobile fractions allows us to calculate the moments of the unbound, bound and total tau protein distributions individually,

$$\langle x^2(t)\rangle_j = \frac{1}{\overline{n}_j(t)} \int_{-\infty}^{\infty} x^2 n_j(x, t)\, dx, \tag{2.7}$$

where j stands for m, im and tot [16]. To shorten the notation, we use $\langle x^2(t)\rangle = \langle x^2(t)\rangle_{tot}$ in the remainder of this work. Using the Laplace inversion of

$$\frac{\partial^2}{\partial k^2} n_{tot}(k, s)\Big|_{k=0} = \langle x^2(s)\rangle, \tag{2.8}$$

we obtain the expression

$$\langle x^2(t)\rangle = 2D_{eff}t + 2D\tau_{im}\frac{f_m\tau_{im}/\tau_m - f_{im}}{(1 + \tau_{im}/\tau_m)^2}\left(1 - e^{-(\tau_m^{-1} + \tau_{im}^{-1})t}\right) \tag{2.9}$$

for the second moment. In the next section, we consider the initial conditions, when all tracers are initially mobile. This is chosen for didactic purposes, as this initial condition shows the plateau in the MSD and intermittent Laplace distribution most clearly. In §4, we consider immobile initial conditions and finally consider equilibrium initial conditions in §5, where the effects discussed in earlier sections are present at the same time.

3. All tracers initially mobile

We now consider the initial condition when all tracers are mobile, i.e. $n_m(x, 0) = \delta(x)$ and $n_{im}(x, 0) = 0$. This initial condition does not correspond to the experiment carried out by Igaev *et al.* [17]. However, this situation could be realized experimentally, e.g. by using the method of injection of fluorescently labelled tau proteins [53]. In what follows, we repeatedly use the time-scale separation $\tau_m \ll \tau_{im}$ observed for tau proteins and also relevant to other systems.

3.1. Concentration

We calculate the densities at short, intermediate and long times. In B.1, we obtain the Gaussian

$$n_{tot}(x, t) \sim \frac{1}{\sqrt{4\pi Dt}} \exp\left(-\frac{x^2}{4Dt}\right) \tag{3.1}$$

in the short-time limit $t \ll \tau_m, \tau_{im}$. The Gaussian (3.1) can be seen in figure 2 in the top left panel. In this figure $n_m(x, t)$,

$n_{\mathrm{tot}}(x,\ t)$ and a histogram are shown. The densities are obtained from Laplace inversions of the expressions in Laplace space (2.3), while the histogram is obtained from simulations, and colours denote the number of immobilization events N_{im}. Initially, all particles are mobile and diffuse freely, as denoted by the black colouring.

The concentration of freely diffusing particles that have not immobilized yet, i.e. have zero immobilization events $N_{\mathrm{im}} = 0$, is given by the PDF of free Brownian motion multiplied by the probability of not having immobilized, i.e.

$$n_{\mathrm{m}}(x,\ t|N_{\mathrm{im}} = 0) = \frac{\exp(-t/\tau_{\mathrm{m}})}{\sqrt{4\pi Dt}} \exp\left(-\frac{x^2}{4Dt}\right). \tag{3.2}$$

These mobile tracers immobilize with the position-dependent rate $n_{\mathrm{m}}(x,\ t\,|\,N_{\mathrm{im}} = 0)/\tau_{\mathrm{m}}$. Integrating from $t' = 0$ to $t' = t$, we obtain in the limit $t \ll \tau_{\mathrm{im}}$ (i.e. at short and intermediate times) that

$$\begin{aligned} n_{\mathrm{im}}(x,\ t \ll \tau_{\mathrm{im}}) &\sim \int_0^t \frac{\exp(-t'/\tau_{\mathrm{m}})/\tau_{\mathrm{m}}}{\sqrt{4\pi Dt'}} \exp\left(-\frac{x^2}{4Dt'}\right) \mathrm{d}t' \\ &= \frac{\exp(-|x|/\sqrt{D\tau_{\mathrm{m}}})}{\sqrt{4D\tau_{\mathrm{m}}}} \frac{1 - \mathrm{erf}\left(|x|/\sqrt{4Dt} - \sqrt{t/\tau_{\mathrm{m}}}\right)}{2} \\ &\quad - \frac{\exp(|x|/\sqrt{D\tau_{\mathrm{m}}})}{\sqrt{4D\tau_{\mathrm{m}}}} \frac{1 - \mathrm{erf}\left(|x|/\sqrt{4Dt} + \sqrt{t/\tau_{\mathrm{m}}}\right)}{2}. \end{aligned} \tag{3.3}$$

Comparing (3.3) with the Laplace inversion of $n_{\mathrm{im}}(x,\ s)$ (2.3) in figure 8, we find very good agreement in the relevant range $t \ll \tau_{\mathrm{im}}$.[2] For the total density, we obtain by adding $n_{\mathrm{m}}(x,\ t)$ (3.1) and $n_{\mathrm{im}}(x,\ t)$ (3.3)

$$n_{\mathrm{tot}}(x,\ t) \sim \frac{\exp(-t/\tau_{\mathrm{m}})}{\sqrt{4\pi Dt}} \exp\left(-\frac{x^2}{4Dt}\right) + n_{\mathrm{im}}(x,\ t \ll \tau_{\mathrm{im}}),$$
$$t \ll \tau_{\mathrm{im}} \tag{3.4}$$

for the full tracer density. For $t \ll \tau_{\mathrm{m}}$, we recover the Gaussian (3.1) from (3.4), while for $\tau_{\mathrm{m}} \ll t \ll \tau_{\mathrm{im}}$ the distribution is distinctly non-Gaussian, as shown in figure 2. Up to around $t = 0.6$ s, the motion of the free tracers is dominated by the Gaussian $n_{\mathrm{m}}(x,\ t\,|\,N_{\mathrm{im}} = 0)$ (see (3.2)), which spreads like free Brownian particles, shown as a white dotted line in figure 2. At around $t = 1.6$ s, most of the tracers with $N_{\mathrm{im}} = 0$ immobilized and the majority of mobile tracers were immobile exactly once ($N_{\mathrm{im}} = 1$) and transitioned back to the mobile zone, as shown by the red area. Because of the immobilization, these tracers have moved less than the free particles with $N_{\mathrm{im}} = 0$ and a Laplace distribution emerges in the centre. For $x \ll t\sqrt{D/\tau_{\mathrm{m}}}$ and $t \gg \tau_{\mathrm{m}}$, we can use the asymptotic $\lim_{x\to\infty} \mathrm{erf}(x) = -\lim_{x\to\infty} \mathrm{erf}(-x) = 1$ in $n_{\mathrm{im}}(x,\ t \ll \tau_{\mathrm{im}})$ (equation (3.3)), and obtain from $n_{\mathrm{tot}}(x,\ t)$ (3.4) the expression

$$n_{\mathrm{tot}}(x,\ t) \sim \frac{1}{\sqrt{4D\tau_{\mathrm{m}}}} \exp\left(-\frac{|x|}{\sqrt{D\tau_{\mathrm{m}}}}\right), \tag{3.5}$$

in the intermediate-time regime $\tau_{\mathrm{m}} \ll t \ll \tau_{\mathrm{im}}$. Combining the conditions $t \ll \tau_{\mathrm{m}}$ and $x \ll t\sqrt{D/\tau_{\mathrm{im}}}$ leads to $x \ll \tau_{\mathrm{im}}\sqrt{D/\tau_{\mathrm{m}}} = 71\ \mu\mathrm{m}$, which is large compared with the standard deviation $\sqrt{2D\tau_{\mathrm{m}}} = 2.1\ \mu\mathrm{m}$ of the Laplace distribution (3.5). This means that the distribution follows such a Laplace shape for a large range of positions. The total concentration, in turn, therefore follows a Laplace distribution with fixed parameters. This is a pronounced deviation from a Gaussian distribution. This result can also be obtained from calculations in Laplace space, as shown in B.2. By contrast, for times significantly longer than τ_{im}, many immobilizations take place, as shown by the bright yellow area in figure 2, where the distribution follows the Gaussian (2.4) with the effective diffusivity $D_{\mathrm{eff}} = D/(1 + \tau_{\mathrm{im}}/\tau_{\mathrm{m}})$.

3.2. Mean squared displacement

From the general expression for the MSD (2.9) for immobile initial conditions, we obtain the expression

$$\langle x^2(t)\rangle = \frac{2D}{1 + \tau_{\mathrm{im}}/\tau_{\mathrm{m}}} \left[t + \frac{\tau_{\mathrm{im}}^2/\tau_{\mathrm{m}}}{1 + \tau_{\mathrm{im}}/\tau_{\mathrm{m}}} \left(1 - \mathrm{e}^{-(\tau_{\mathrm{m}}^{-1} + \tau_{\mathrm{im}}^{-1})t}\right)\right]. \tag{3.6}$$

At intermediate times, the MSD (expression (3.6)) exhibits a plateau-like behaviour with the constant MSD

$$\langle x^2(t)\rangle \sim 2D\tau_{\mathrm{m}}, \quad \tau_{\mathrm{m}} \ll t \ll \tau_{\mathrm{im}}, \tag{3.7}$$

corresponding to free Brownian particles that moved for the duration τ_{m}. This requires the condition $\tau_{\mathrm{m}} \ll \tau_{\mathrm{im}}$, which is satisfied in the tau protein case [17], with $\tau_{\mathrm{m}} = 0.16$ s and $\tau_{\mathrm{im}} = 7.7$ s. Such plateaus are often found when tracers diffuse in porous media or for dynamics in crowded membranes or environments with obstacles, in which the tracer can be transiently confined [38,46,48,54,55]. The MSD (3.6) is shown in figure 3*a* as the black solid line.

When calculating the moments of the mobile and immobile tracers (2.7), the time-dependent normalizations of the tracer densities (2.6),

$$\overline{n}_{\mathrm{m}}(t) = \frac{\tau_{\mathrm{m}}}{\tau_{\mathrm{m}} + \tau_{\mathrm{im}}} \left[\frac{1 + \tau_{\mathrm{im}}}{\tau_{\mathrm{m}}\,\mathrm{e}^{-(\tau_{\mathrm{m}}^{-1} + \tau_{\mathrm{im}}^{-1})t}}\right] \tag{3.8}$$

and

$$\overline{n}_{\mathrm{im}}(t) = \frac{\tau_{\mathrm{im}}}{\tau_{\mathrm{m}} + \tau_{\mathrm{im}}} [1 - \mathrm{e}^{-(\tau_{\mathrm{m}}^{-1} + \tau_{\mathrm{im}}^{-1})t)}], \tag{3.9}$$

need to be taken into account, yielding the moments of the mobile and immobile densities (2.7) [16]

$$\begin{aligned} \langle x^2(t)\rangle_{\mathrm{m}} = \frac{2D}{(1 + \tau_{\mathrm{im}}/\tau_{\mathrm{m}})(1 + \tau_{\mathrm{im}}/\tau_{\mathrm{m}}\,\mathrm{e}^{-(\tau_{\mathrm{m}}^{-1} + \tau_{\mathrm{im}}^{-1})t})} \Bigg[t\left(1 + \frac{\tau_{\mathrm{im}}^2}{\tau_{\mathrm{m}}^2}\,\mathrm{e}^{-(\tau_{\mathrm{m}}^{-1} + \tau_{\mathrm{im}}^{-1})t}\right) \\ + \frac{2\tau_{\mathrm{im}}^2/\tau_{\mathrm{m}}}{1 + \tau_{\mathrm{im}}/\tau_{\mathrm{m}}}(1 - \mathrm{e}^{-(\tau_{\mathrm{m}}^{-1} + \tau_{\mathrm{im}}^{-1})t})\Bigg] \end{aligned} \tag{3.10}$$

and

$$\begin{aligned} \langle x^2(t)\rangle_{\mathrm{im}} = \frac{2D}{1 - \mathrm{e}^{-(\tau_{\mathrm{m}}^{-1} + \tau_{\mathrm{im}}^{-1})t}} \Bigg[\frac{t}{1 + \tau_{\mathrm{im}}/\tau_{\mathrm{m}}}\left(1 - \frac{\tau_{\mathrm{im}}}{\tau_{\mathrm{m}}}\,\mathrm{e}^{-(\tau_{\mathrm{m}}^{-1} + \tau_{\mathrm{im}}^{-1})t}\right) \\ + \frac{\tau_{\mathrm{im}}^2/\tau_{\mathrm{m}} - \tau_{\mathrm{im}}}{(1 + \tau_{\mathrm{im}}/\tau_{\mathrm{m}})^2}\left(1 - \mathrm{e}^{-(\tau_{\mathrm{m}}^{-1} + \tau_{\mathrm{im}}^{-1})t}\right)\Bigg]. \end{aligned} \tag{3.11}$$

As shown in figure 3, the mobile second moment exhibits a peak at around $t = 0.6$ s, followed by a plateau. This peak arises as the density of mobile tracers initially consists of mobile tracers that have never immobilized. Once $t \gg \tau_{\mathrm{m}}$, the mobile density mainly consists of tracers that were immobile (at least) once and mobilized, as discussed above. Since the latter had less time to move, they have spread less and the MSD temporarily decreases.

The immobile MSD (3.11) has the short-time behaviour $\langle x^2(t)\rangle_{\mathrm{im}} \sim Dt$ for $t \ll \tau_{\mathrm{m}},\ \tau_{\mathrm{im}}$. The factor $\frac{1}{2}$ when compared

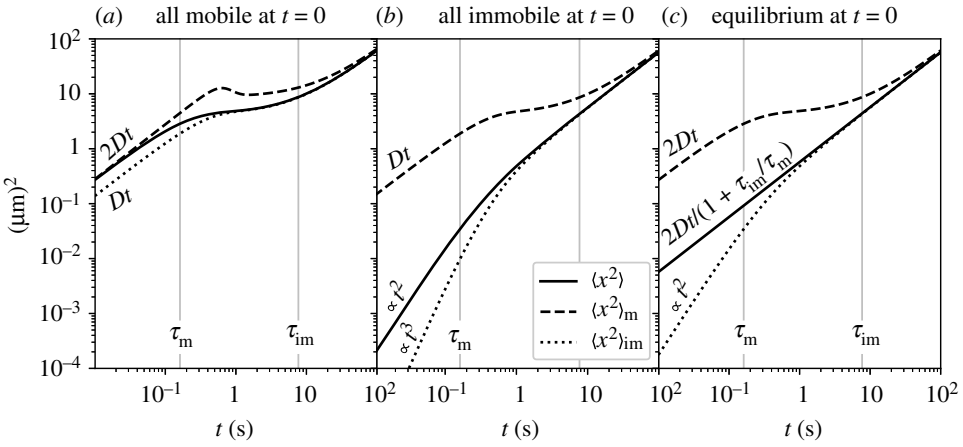

Figure 3. Second moments for different initial conditions on a log–log scale. In (*a*), all tracers are initially mobile, as in §3. After a linear growth, the second moment $\langle x^2(t)\rangle$ of all tracers (equation (3.6)) shows a plateau for $\tau_m \ll t \ll \tau_{im}$. The second moment of the mobile particles (equation (3.10)) in (*a*) has a peak immediately before the total particle moment and the mobile particle moment reach a plateau value. Immobile tracers spread $\sim Dt$ at short times, and the second moment (3.11) has a plateau at intermediate times. In (*b*), all tracers are initially immobile, as in §4. The second moment of all tracers (equation (4.3)) grows $\sim Dt^2/\tau_{im}$ at short times, owing to the decaying number of particles located at $x = 0$. The immobile tracers spread $\sim Dt^3/(3\tau_m\tau_{im})$ at short times, while the full expression is given in equation (4.3). The mobile tracers in (*b*) spread exactly like the immobile tracers in (*a*), where all tracers are initially mobile. (*c*) The equilibrium case, §5, in which the second moment grows like $2Dt/(1 + \tau_{im}/\tau_m)$ (equation (5.3)) for all times. The mobile and immobile moments exactly match the moments of the total distribution with mobile and immobile initial conditions, respectively.

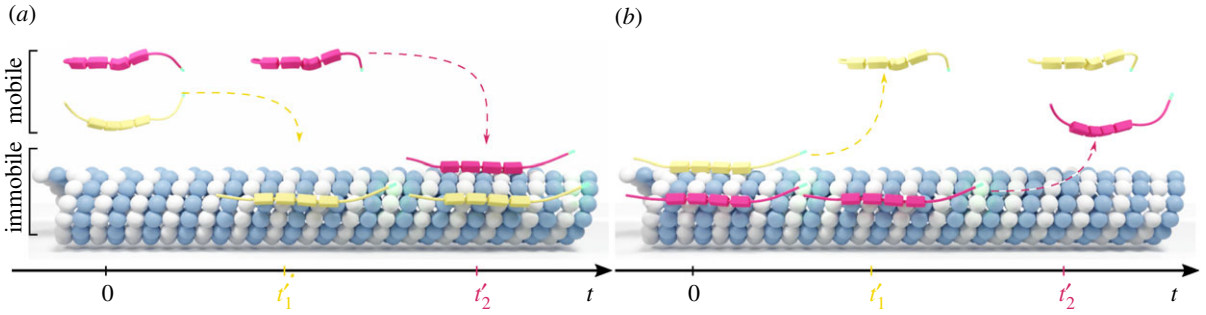

Figure 4. Schematic showing the short-time behaviour of tracers for mobile (*a*) and immobile initial conditions (*b*) at three snapshots of time. In both panels, the tracers change the mobilization state at times t'_1 and t'_2, respectively. For mobile initial conditions in (*a*), the number of immobile tracers grows $\sim t/\tau_m$ at short times. Namely, the later a tracer immobilizes, the longer it was previously mobile. In (*b*), the number of mobile tracers grows $\sim t/\tau_{im}$. Namely, the earlier a tracer mobilizes in (*b*), the longer it is mobile.

with the mobile tracers arises because immobile tracers effectively average over the history of the mobile tracers. Namely, for $t' \ll \tau_m, \tau_{im}$, mobile particles immobilize with the constant rate $p(t') = 1/\tau_m$. A particle that immobilized at time t' before moved for the duration t' and thus contributes $2Dt'$ to the second moment for $t > t'$; see figure 4*a* for a schematic drawing. When averaging over different mobile periods t' and normalizing with the fraction of immobile tracers $\int_0^t p(t')dt'$, we obtain

$$\langle x^2(t)\rangle_{im} \sim 2D\frac{\int_0^t t'p(t')\,dt'}{\int_0^t p(t')\,dt'} = \frac{2D\int_0^t t'/\tau_m\,dt'}{t/\tau_m} = Dt, \quad \text{for } t \ll \tau_m, \tau_{im}. \tag{3.12}$$

As mentioned above, the long-time limits of the MSDs of all densities remain equal to $2D_{eff}t$, regardless of the fractions f_m and f_{im}.

4. All tracers initially immobile

We now discuss the case when all tracers are immobile at $t = 0$, $n_{im}(x, 0) = \delta(x)$ and $n_m(x, 0) = 0$.

4.1. Concentration

In B.1, we obtain the short-time behaviour

$$n_{tot}(x, t) \sim \frac{2t/\tau_{im}}{\sqrt{4\pi Dt}}\,e^{-(x^2/4Dt)} - \frac{|x|\left(1 - \mathrm{erf}\left(\frac{|x|}{\sqrt{4Dt}}\right)\right)}{2D\tau_{im}} + \left(1 - \frac{t}{\tau_{im}}\right)\delta(x), \quad \text{for } t \ll \tau_m, \tau_{im} \tag{4.1}$$

by applying approximations for large s in Laplace space. Expression (4.1) is shown in the left panel of figure 5 as the black dashed line. In particular, note the distinctively non-Gaussian shape of the distribution in contrast to the case of mobile initial conditions. The Gaussian in equation (4.1) has the normalization $\sim 2t/\tau_{im}$, while the second term has the normalization $\sim -t/\tau_{im}$, and thus the whole expression (4.1) is normalized to unity. In B.2, we obtain the total density at intermediate times $\tau_m \ll t \ll \tau_{im}$

$$n_{tot}(x, t) \sim \frac{t/\tau_{im}}{\sqrt{4D\tau_m}}\exp\left(-\frac{|x|}{\sqrt{D\tau_m}}\right) + \left(1 - \frac{t}{\tau_{im}}\right)\delta(x), \tag{4.2}$$

as shown in figure 5 in the top row (except for the leftmost panel) as a black–white striped line. Compared with the mobile initial

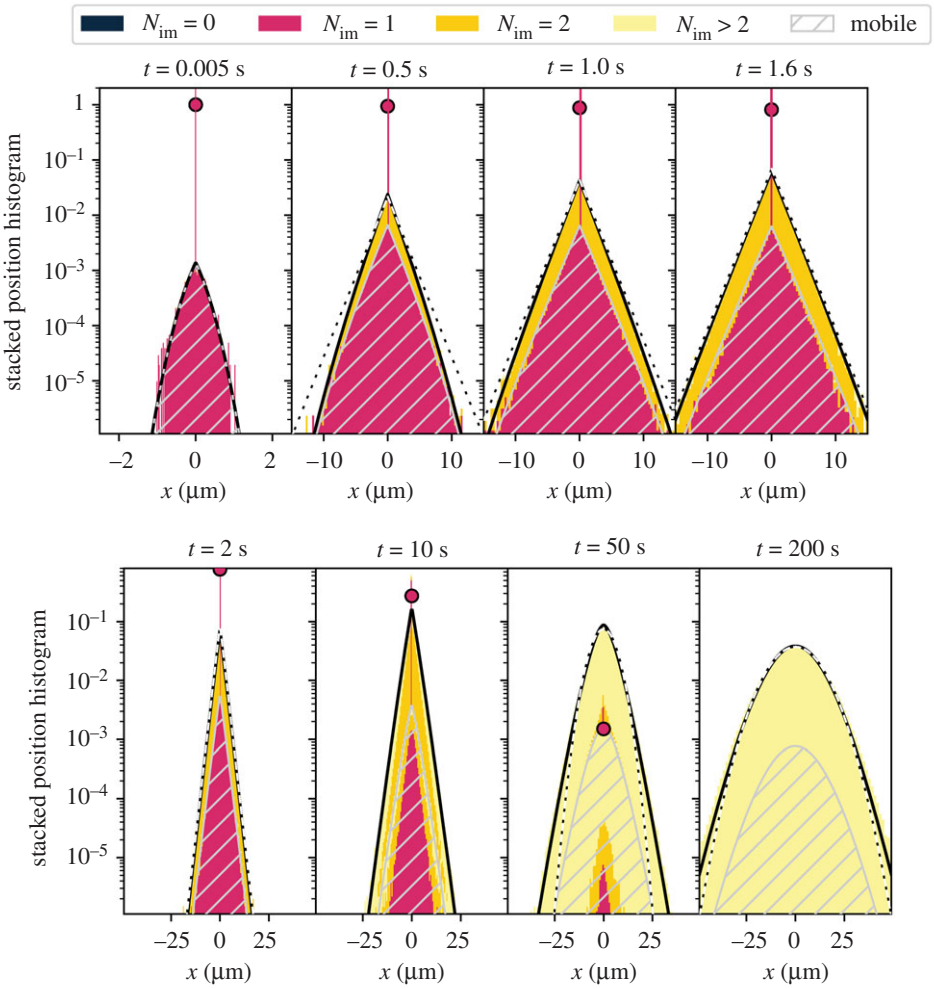

Figure 5. Concentration profiles for immobile initial conditions; for a description of the legend, see figure 2. The main difference from the case of mobile initial conditions poses the peak of immobile tracers at $x = 0$ that have not moved up to time t, as shown by the circle. In addition, we here find a pronounced relative increase of mobile particle numbers and the very slow spread of immobile tracers at short times. The short-time approximation (4.1) is shown as the black dashed line in the top left panel. For $t = 0.5$–10 s, the white dashed line shows the Laplacian (4.2) with growing weight; for $t = 50$ s and 200 s, it shows the long-time Gaussian (2.4).

condition, the coefficient of the Laplace distribution has the linear growth t/τ_{im}. Most tracers remain immobile at the origin at $t = 1.6$ s. In B.4, we find expression (B 11) for $n_{tot}(x, t)$, which is valid for $t \ll \tau_{im}$ and contains equations (4.1) and (4.2) as limits. In figure 5, the lower panels show the transition from the Laplace distribution to the Gaussian (2.4).

4.2. Mean squared displacement

From the general expression for the MSD (2.9), we obtain the expression

$$\langle x^2(t)\rangle = \frac{2D}{1+\tau_{im}/\tau_m}\left[t - \frac{\tau_{im}}{1+\tau_{im}/\tau_m}\left(1 - e^{-(\tau_m^{-1}+\tau_{im}^{-1})t}\right)\right]. \tag{4.3}$$

The MSD (4.3) has the ballistic short-time behaviour

$$\langle x^2(t)\rangle \sim \frac{Dt^2}{\tau_{im}} + O(t^3), \quad t \ll \tau_m, \tau_{im}. \tag{4.4}$$

The Landau symbol $O(\cdot)$ represents higher order terms. The ballistic behaviour at short times $t \ll \tau_{im}$ arises because the fraction $\exp(-t/\tau_{im}) \sim 1 - t/\tau_{im}$ of tracers are immobile at $x = 0$ and hence do not contribute to the second moment. For $t' \ll \tau_m \ll \tau_{im}$, immobile particles mobilize with the constant rate $p(t') = 1/\tau_{im}$. A particle that mobilized at time t' moved for the duration $t - t'$ and thus contributes $2D(t - t')$ to the second moment for $t > t'$; see figure 4*a* for a schematic drawing. When integrating over different mobilization times t', we find

$$\langle x^2(t)\rangle \sim 2D\int_0^t (t-t')p(t')\,dt' = 2D\int_0^t \frac{t-t'}{\tau_{im}}\,dt' = D\frac{t^2}{\tau_{im}}, \quad t \ll \tau_m \ll \tau_{im}. \tag{4.5}$$

We obtain the number of free and bound tracers from the general expression (2.6),

$$\overline{n}_m(t) = \frac{\tau_m}{\tau_m+\tau_{im}}\left[1 - e^{-(\tau_m^{-1}+\tau_{im}^{-1})t)}\right] \tag{4.6}$$

and

$$\overline{n}_{im}(t) = \frac{\tau_{im}}{\tau_m+\tau_{im}}\left[\frac{1+\tau_m}{\tau_{im}\,e^{-(\tau_m^{-1}+\tau_{im}^{-1})t}}\right]. \tag{4.7}$$

This produces the normalization of the immobile moment, and we find

$$\langle x^2(t)\rangle_{im} = \frac{2Dt}{1+\tau_m/\tau_{im}}\frac{1+e^{-(\tau_m^{-1}+\tau_{im}^{-1})t}}{\tau_{im}/\tau_m + e^{-(\tau_m^{-1}+\tau_{im}^{-1})t}} - \frac{4D\tau_{im}^2/\tau_m}{(1+\tau_{im}/\tau_m)^2}\frac{1-e^{-(\tau_m^{-1}+\tau_{im}^{-1})t}}{\tau_{im}/\tau_m + e^{-(\tau_m^{-1}+\tau_{im}^{-1})t}}. \tag{4.8}$$

This MSD has the short-time behaviour $\langle x^2(t)\rangle_{\rm im} \sim Dt^3/(3\tau_{\rm im}\tau_{\rm m})$ for $t \ll \tau_{\rm m}, \tau_{\rm im}$. The cubic scaling emerges as the only immobile tracers, which are not located at the origin, have previously mobilized and then immobilized again. The mobile concentration grows $\sim t/\tau_{\rm im}$ at short times $t \ll \tau_{\rm im}$. Integrating over the time t' spent in the mobile phase yields the cubic scaling

$$\langle x^2(t)\rangle_{\rm im} \sim 2D\int_0^t \frac{1}{\tau_{\rm m}} n_{\rm m}(t-t')t'\,{\rm d}t' = \frac{2D}{\tau_{\rm m}\tau_{\rm im}}\int_0^t (t-t')t'\,{\rm d}t' = D\frac{t^3}{3\tau_{\rm m}\tau_{\rm im}}, \tag{4.9}$$

where, in the first step, we took the limit $t \ll \tau_{\rm m}$. Since the mobile concentration with immobile initial conditions is proportional to the immobile concentration with mobile initial conditions, $\langle x^2(t)\rangle_{\rm m}$ is equal to $\langle x^2(t)\rangle_{\rm im}$ in (3.11) with mobile initial conditions. This can be seen in figure 3*a*,*b*. As for the mobile initial condition considered in §3, the MSDs of all densities grow $\sim 2D_{\rm eff}t$ asymptotically.

5. Equilibrium initial fractions of initial mobile tracers

In this section, we use the equilibrium values $n_{\rm m}(x,0) = f_{\rm m}^{\rm eq}\delta(x)$ and $n_{\rm im}(x,0) = f_{\rm im}^{\rm eq}\delta(x)$ as initial conditions.

5.1. Concentration profiles

From the general expressions (2.1) and (2.3) for the densities $n_{\rm m}(x,s)$ and $n_{\rm tot}(x,s)$, we find that the mobile concentration of the equilibrium case discussed here is proportional to the total concentration for the mobile initial condition in §3 at all times. To understand why this is true, we note that both concentrations at all times contain mobile tracers that were initially mobile. Moreover, from equations (2.1) and (2.3), we see that the mobile concentration of the equilibrium case contains initially immobile tracers, while the total concentration contains immobile tracers that were initially mobile. In equations (2.1) and (2.3), the respective terms that appear in addition to the initially mobile fractions that are still mobile are proportional to each other at all times, as described in §2.1. An analogous relation holds between the immobile concentration with equilibrium initial conditions and the total concentration with immobile initial conditions, as can be seen in equations (2.1) and (2.3).

We consider the short-time approximation $t \ll \tau_{\rm m}, \tau_{\rm im}$ for which initially immobile tracers have not yet mobilized and initially mobile tracers have not yet been trapped. Therefore, we can neglect the terms with the rates $\tau_{\rm m}^{-1}$ and $\tau_{\rm im}^{-1}$ in (1.2) and solve $n_{\rm m}(x,t)$ and $n_{\rm im}(x,t)$ separately, yielding

$$n_{\rm tot}(x,t) \sim \frac{f_{\rm m}^{\rm eq}}{\sqrt{4\pi Dt}}\exp\left(-\frac{x^2}{4Dt}\right) + f_{\rm im}^{\rm eq}\delta(x), \quad t \ll \tau_{\rm m}, \tau_{\rm im}, \tag{5.1}$$

with a Gaussian distribution describing free diffusion in addition to a Dirac-δ distribution of initially immobile tracers that have not yet moved. This behaviour can be seen in the top left panel of figure 6. The same result as (5.1) can be obtained by combining the short-time expressions for the mobile (3.1) and immobile (4.1) initial conditions for $t \ll \tau_{\rm m}, \tau_{\rm im}$, as done in equation (B 5). At short times, the total density (5.1) behaves like the case of mobile initial conditions with an additional delta peak. At intermediate times $\tau_{\rm m} \ll t \ll \tau_{\rm im}$, we obtain

$$n_{\rm tot}(x,t) \sim \frac{t/\tau_{\rm im}}{\sqrt{4D\tau_{\rm m}}}\exp\left(-\frac{|x|}{\sqrt{D\tau_{\rm m}}}\right) + \left(1-\frac{t}{\tau_{\rm im}}\right)\delta(x) \tag{5.2}$$

by combining the mobile (3.5) and immobile expression (4.2), respectively.[3] In fact equation (5.2) is the same as expression (4.2) for the case of immobile initial conditions, in the intermediate-time regime. This result is shown in figure 6, where this approximation is compared with the full concentration from $t = 0.5$ to $t = 2$. This result is the one-dimensional equivalent to the findings in [32]. The lower right panels of figure 6 show the Gaussian long-time limit (2.4) as a black–white striped line.

5.2. Mean squared displacement

The number of mobile and immobile tracers remains constant for equilibrium initial conditions. At all times, the second moment of all tracers (2.9) thus simplifies to

$$\langle x^2(t)\rangle = \frac{2D}{1+\tau_{\rm im}/\tau_{\rm m}}t. \tag{5.3}$$

The second moment is similar to that of a free Brownian particle, with the effective diffusion coefficient $D_{\rm eff} = D/(1+\tau_{\rm im}/\tau_{\rm m})$, as shown in figure 3. This is a known result from models for Fickian yet non-Gaussian diffusion [32]. The mobile and immobile moments, $\langle x^2(t)\rangle_{\rm m}$ and $\langle x^2(t)\rangle_{\rm im}$, are equivalent to the moments of the full density with mobile (3.6) and immobile (4.3) initial conditions, as can be seen in figure 3. This relation holds because the respective densities are proportional, as discussed above. The mobile and immobile moments show clear anomalous diffusion for $t \ll \tau_{\rm im}$, with a quite long crossover dynamics, as depicted in figure 3*c*. The mobile moment has a plateau in the intermediate regime $\tau_{\rm m} \ll t \ll \tau_{\rm im}$ and the immobile moment behaves ballistically at short times $t \ll \tau_{\rm m}$.

In the long-time limit, all mobile and immobile second moments grow like the moments of the total concentration, i.e. $\langle x^2(t)\rangle_{\rm m} \sim \langle x^2(t)\rangle_{\rm im} \sim 2D_{\rm eff}t$ for $t \gg \tau_{\rm im}, \tau_{\rm m}$.

6. Discussion and conclusion

We considered a quite simple mobile–immobile model according to which tracer particles switch between a mobile diffusing state and an immobilized state. On average, the tracers remain mobile for the duration $\tau_{\rm m}$ and immobile for $\tau_{\rm im}$. We considered the particular case, motivated by experiments on tau proteins binding to and unbinding from microtubules in axons of dendritic cells [17], when the two time scales are separated, $\tau_{\rm m} \ll \tau_{\rm im}$. We analysed three different initial conditions with varying fractions of mobile to immobile tracers at the origin, which can, in principle, all be realized in experiments. The initial condition of mobile tracers can be realized by injecting fluorescently labelled proteins [53]. Initially, immobile tracers could in principle be obtained in single-particle tracking experiments, by focusing on the tracks of immobile tracers. Equilibrium fractions of mobile tracers naturally occur when the tau proteins were in proximity to the microtubules for $t \gg \tau_{\rm m}, \tau_{\rm im}$ before the start of the data acquisition.

First, we studied the case when all tracers are initially mobile, as described in the experiment in [53]. Second, we assumed all tracers to be initially immobile. Third, we considered an equilibrium fraction, corresponding to the experiment in [17]. For non-equilibrium fractions of initially mobile

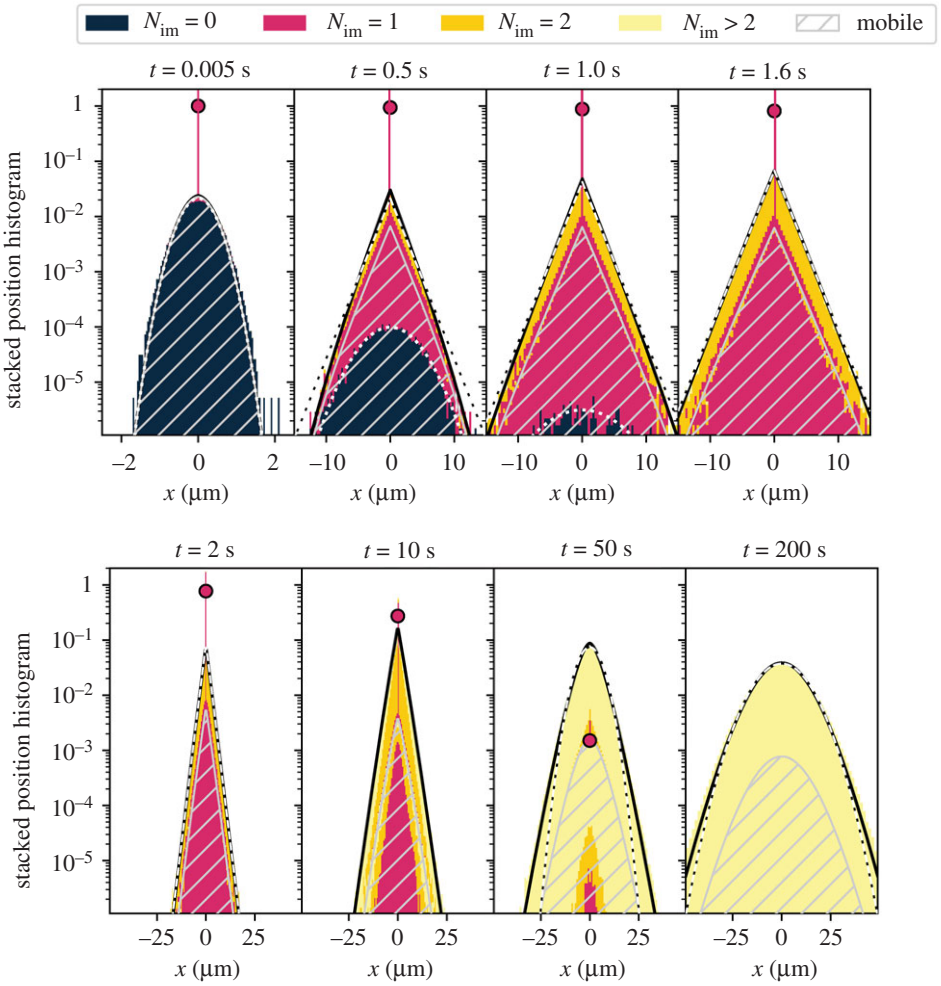

Figure 6. Concentration profiles for equilibrium initial conditions. At $t = 0$, all tracers are at $x = 0$ and the equilibrium fraction $\tau_{im}/(\tau_m + \tau_{im})$ is immobile. For a description of the legend, see figure 2. The top left panel shows the short-time behaviour consisting of a Gaussian and a δ-distribution (equation (5.1)). At $t = 1$, almost all initially mobile tracers immobilized at least once and the total concentration follows the Laplace distribution (5.2), as shown by the black–white striped line for $t = 0.5$–2 s. At longer times, after several immobilizations the concentration profiles cross over to a Gaussian, as witnessed by equation (2.4), shown as a black–white striped line for $t = 50$ s and $t = 200$ s.

tracers, we find anomalous diffusion at short and intermediate time scales, at which initially mobile tracers display a plateau in the MSD at intermediate times and initially immobile tracers spread ballistically at short times. At $t \ll \tau_m$ and an initial equilibrium fraction, the tracer density consists of a Gaussian and a delta peak. Initially, mobile tracers follow a Gaussian distribution at short times. When all tracers are initially immobile, the short-time distribution consists of a delta peak and a non-Gaussian distribution. At intermediate times $\tau_m \ll t \ll \tau_{im}$, the distribution is made up of a Laplace distribution and a delta distribution of initially immobile tracers that have not moved yet. The coefficients of the two distributions depend on the specific initial conditions. We additionally obtain expressions for the densities that are valid for the whole range $t \ll \tau_{im}$. We stress that the distribution is non-Gaussian at intermediate times, regardless of the initial conditions. By contrast, the distribution asymptotically at long times matches a Gaussian for all initial conditions. The densities of mobile and immobile tracers with equilibrium initial conditions match the total tracer densities of mobile and immobile initial conditions, respectively, at all times. Moreover, the immobile tracer density from mobile initial conditions is proportional to the mobile tracer density from immobile initial conditions at all times. As a special case for equilibrium initial conditions, our model corresponds to the one-dimensional version of the model used in [32] to describe Fickian yet non-Gaussian diffusion. We find the same linear MSD for all times and obtain a closed expression for the Laplace distribution at intermediate time scales.

The model developed here is, of course, much more general. We provided the framework for any ratio of the characteristic time scales τ_m and τ_{im}, such that the model will be useful for scenarios ranging from geophysical experiments with Poissonian (im)mobilization statistics to molecular systems such as protein (un)binding to DNA in nanochannel set-ups. To the best of our knowledge, the transient Laplace distribution of tau proteins has not been observed yet. We now discuss possible experiments that could reveal the anomalous diffusion regime and the Laplace distribution, which depend on the time scales τ_m and τ_{im}. For the present analysis, we used the parameters $\tau_m = 0.16$ s and $\tau_{im} = 7.7$ s for tau proteins, which were obtained from an FDAP experiment [17]. FDAP experiments do not directly allow the observation of single-particle displacement densities and the moments thereof. However, a single-molecule tracking (SMT) study of tau proteins [18] with two-dimensional trajectories of 2.2 s length was conducted, where we expect the transient Laplace distribution to be visible in the marginal distribution, given that the sample size is large enough. From SMT experiments, the moments can be obtained, although, in [18], the moments of the distribution were not evaluated. Another example for a system with $\tau_{im} > \tau_m$ is given by synaptic vesicles [19]. In [19], fluorescence correlation spectroscopy reveals $\tau_{im} = (4.2 \pm 0.4)$ s and $\tau_m = (2.0 \pm 0.4)$ s. In addition,

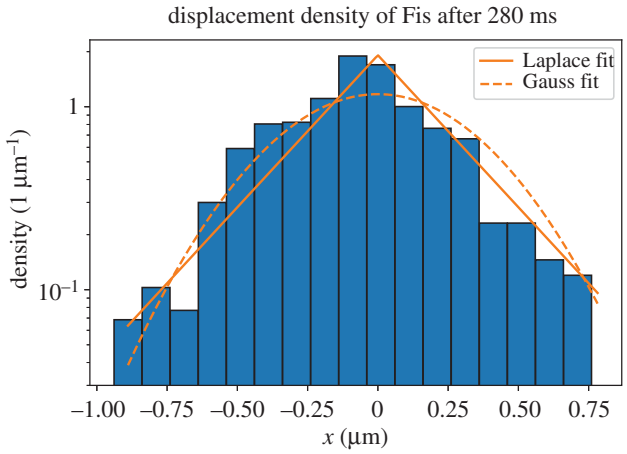

Figure 7. Displacement distribution of the Fis DNA-binding protein. The histogram depicts the data measured by Kamagata *et al.* [29]. The solid and dashed lines depict fits with a Laplace and a Gaussian distribution, respectively. The Laplace fit $\exp(-|x|/a)/2a$ yields $a = 0.27\ \mu$m. The Gaussian fit $\exp(-x^2/(4Dt))/\sqrt{4\pi Dt}$ with $t = 0.28$ s yields $D = 0.21\ \mu\text{m}^2\,\text{s}^{-1}$, which is within the margin of error of the value $(0.19 \pm 0.02)\ \mu\text{m}^2\,\text{s}^{-1}$ of the fast diffusion coefficient reported in [29]. The data were extracted from the PDF file of [29].

glucocorticoid receptors show long immobilization events with $\tau_{\text{im}} = 13$ ms compared with $\tau_{\text{m}} = 2$ ms, as revealed by fluorescent recovery after a photobleaching experiment [20]. The Laplace distribution cannot be observed in this experiment, owing to the missing information on single tracers. SMT experiments of the transcription factor p53 [22] show a switched separation of time scales with $\tau_{\text{im}} = 1.80$ s and $\tau_{\text{m}} = 8.4$ s. Here, SMT allows us to measure the exponential binding time distribution corresponding to a single binding rate, as in our model. The second moment is measured for up to 0.6 s, where longer trajectories would allow for a comprehensive comparison with the moments calculated in this work. For $\tau_{\text{m}} > \tau_{\text{im}}$, the Laplace distribution does not arise. We now look at another SMT experiment in more detail. In [29], the architectural DNA-binding protein Fis was observed to have a linear MSD and a non-Gaussian displacement distribution, as depicted in figure 7. The authors of [29] fitted two Gaussians to the distribution and deduced the presence of two sliding modes of Fis on the DNA. Since the motion during the slow sliding mode is within experimental accuracy, it is plausable to assume that the non-Gaussian distribution emerges as a result of immobilization. In figure 7, we show fits with a Laplace distribution and a Gaussian distribution in a logarithmic presentation. The Laplace distribution matches the general shape with few exceptions around $-0.4\ \mu$m, while the Gaussian distribution does not capture the peak in the centre. We note that the Laplace distribution requires a single fitting parameter, compared with the two Gaussians with advection used in [29] requiring five parameters. The apparent Laplace distribution and linear MSD translate to equilibrium initial conditions in our model.

We note that (non-)exponential (im)mobilization has been studied using a Langevin equation with switching diffusivities [56,57] and the continuous time random walk framework, where the waiting time probability distribution function consists of a combination of two exponentials with different time scales [58]. It will be a topic of future research to study the effect of a drift velocity on the pre-asymptotic behaviour for different initial conditions, as well as what happens when non-exponential (im)mobilization is considered in a mobile–immobile model in connection with chemical reactions.

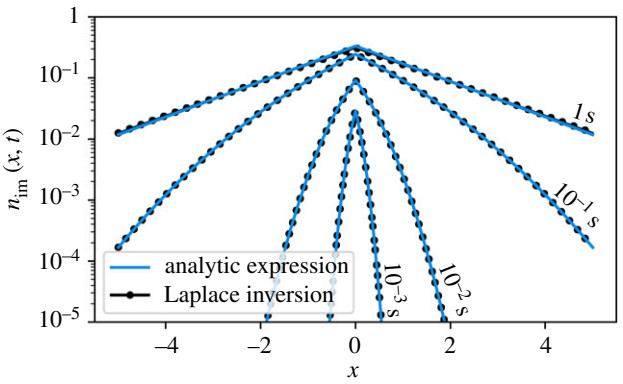

Figure 8. Comparison of the Laplace inversion of $n_{\text{im}}(x, s)$ (expression (2.3)) and the analytic expression for $n_{\text{im}}(x, t)$ (equation (3.3)) that holds for $t \ll \tau_{\text{im}}$. Both overlap almost perfectly for $t < \tau_{\text{im}} = 7.7$ s.

Data accessibility. This article has no addition data.

Authors' contributions. T.J.D.: formal analysis, investigation, methodology, validation, visualization, writing—original draft, writing—review and editing; A.V.C.: conceptualization, formal analysis, investigation, supervision, writing—review and editing; R.M.: conceptualization, funding acquisition, project administration, supervision, validation, writing—original draft, writing—review and editing. All authors gave final approval for publication and agreed to be held accountable for the work performed herein.

Conflict of interest declaration. We declare we have no competing interests.

Funding. We acknowledge funding from the German Science Foundation (DFG, grant no. ME 1535/12-1). A.V.C. acknowledges the support of the Polish National Agency for Academic Exchange (NAWA).

Endnotes

[1]The slow directed motion only plays a role when very long times are considered [17,51,52].

[2]Equations (3.2) and (3.3) can also be obtained by taking the limit $\tau_{\text{im}} \to \infty$ in (1.2) and solving the equations directly.

[3]An approximation for the whole range of $t \ll \tau_{\text{im}}$ can be obtained for any fractions of initially mobile tracers f_{m} by combining equations (3.4) and (B 11) from the mobile and immobile initial conditions, respectively. This yields equation (B 12) and is shown in figure 10.

Appendix A. General equations

Starting with equation (1.2), we apply the Fourier–Laplace transform $f(k, s) = \int_{-\infty}^{\infty}\int_{0}^{\infty} \mathrm{e}^{-st+ikx} f(x, t)\,\mathrm{d}t\mathrm{d}x$ to the rate to obtain

$$\left.\begin{aligned} n_{\text{m}}(k, s) &= \tfrac{f_{\text{m}}+f_{\text{im}}(1/(1+s\tau_{\text{im}}))}{\phi(s)+k^2D} \\ \text{and} \qquad n_{\text{im}}(k, s) &= \tfrac{\tau_{\text{im}}}{1+s\tau_{\text{im}}}\left(f_{\text{im}} + \tau_{\text{m}}^{-1}\,\tfrac{f_{\text{m}}+f_{\text{im}}(1/(1+s\tau_{\text{im}}))}{\phi(s)+k^2D}\right) \end{aligned}\right\} \quad \text{(A 1)}$$

as well as

$$\begin{aligned} n_{\text{tot}}(k, s) &= n_{\text{m}}(k, s) + n_{\text{im}}(k, s) \\ &= \frac{f_{\text{m}} + f_{\text{im}}(1/(1+s\tau_{\text{im}}))}{s}\,\frac{\phi(s)}{\phi(s)+k^2D} \\ &\quad + f_{\text{im}}\frac{\tau_{\text{im}}}{1+s\tau_{\text{im}}} \end{aligned} \quad \text{(A 2)}$$

with $\phi(s) = s[1 + \tau_{\text{im}}\tau_{\text{m}}^{-1}/(1 + s\tau_{\text{im}})]$.

Appendix B. Asymptotics calculated in Laplace space

We go from a short-time limit to a long-time limit.

B.1. Short-time limit

For $t \ll \tau_m$, τ_{im}, we obtain $s\tau_{im} \gg 1$ and $s\tau_{im} \gg 1$. This yields $\phi(s) \sim s$ in this limit. With (A 1) for $f_m = 1$ and $f_{im} = 0$, we obtain the expression

$$n_m(k, s) \sim n_{tot}(k, s) \sim \frac{1}{s + k^2 D}, \tag{B 1}$$

which produces the Gaussian (3.1). We now consider $f_{im} = 1$ and $f_m = 0$ and obtain the expression

$$n_{tot}(k, s) \sim \frac{1}{s\tau_{im}} \frac{1}{s + k^2 D} + \left(\frac{1}{s} - \frac{1}{s^2 \tau_{im}}\right) \tag{B 2}$$

from (A 2) in the limit $s\tau_m \gg 1$ and $s\tau_{im} \gg 1$. Fourier–Laplace inversion yields the expression

$$n_{tot}(x, t) \sim \frac{1}{\tau_{im}} \int_0^t \frac{1}{\sqrt{4\pi D t'}} e^{-(x^2/4Dt')} \, dt' + (1 - t/\tau_{im})\delta(x)$$
$$\text{for } t \ll \tau_m \ll \tau_{im}. \tag{B 3}$$

Solving the integral in (B 3) gives the expression

$$n_{tot}(x, t) \sim \frac{2t/\tau_{im}}{\sqrt{4\pi D t}} e^{-(x^2/4Dt)} - \frac{|x|(1 - \mathrm{erf}(|x|/\sqrt{4Dt}))}{2D\tau_{im}} + \left(1 - \frac{t}{\tau_{im}}\right)\delta(x), \quad \text{for } t \ll \tau_m \ll \tau_{im}, \tag{B 4}$$

where normalization is conserved. By combining expression (B 4) for immobile initial conditions and (3.1) for mobile initial conditions, we obtain the expression

$$n_{tot}(x, t) \sim \left(\frac{f_m + 2f_{im}t}{\tau_{im}}\right) \frac{1}{\sqrt{4\pi D t}} e^{-(x^2/4Dt)} - f_{im} \frac{|x|\left(1 - \mathrm{erf}\left(\frac{|x|}{\sqrt{4Dt}}\right)\right)}{2D\tau_{im}} + f_{im}\left(1 - \frac{t}{\tau_{im}}\right)\delta(x), \tag{B 5}$$

for $t \ll \tau_m \ll \tau_{im}$ for arbitrary fractions of initially mobile tracers.

B.2. Density at intermediate time scales

We now investigate the intermediate time $\tau_m \ll t \ll \tau_{im}$, corresponding to $s\tau_m \ll 1$ and $s\tau_{im} \gg 1$. In this regime, we have $\phi(s) \sim \tau_m^{-1}$, yielding the expression

$$n_{tot}(x, s) \sim \frac{f_m + f_{im}\frac{1}{s\tau_{im}}}{s} \frac{1}{\sqrt{4D\tau_m}} e^{-(|x|/\sqrt{D\tau_m})} + f_{im}\left(\frac{1}{s} - \frac{1}{s^2\tau_{im}}\right)\delta(x) \tag{B 6}$$

from (2.3) for the total concentration. The inverse Laplace transform of (B 6) yields the expression

$$n_{tot}(x, s) \sim \left(\frac{f_m + f_{im}t}{\tau_{im}}\right) \frac{1}{\sqrt{4D\tau_m}} e^{-(|x|/\sqrt{D\tau_m})} + f_{im}\left(\frac{1 - t}{\tau_{im}}\right)\delta(x) \tag{B 7}$$

for $\tau_m \ll t \ll \tau_{im}$.

B.3. Density in the long-time limit

We obtain the long-time limit $t \gg \tau_m$, τ_{im} from $n_{tot}(k, s)$ (A 2) using $s \ll 1/\tau_{im}$, $1/\tau_m$ and $\phi(s) \sim s(1 + \tau_{im}/\tau_{im})$. This yields the expression

$$n_{tot}(x, t) \sim \frac{1}{\sqrt{4\pi D_{eff} t}} e^{-(x^2/4D_{eff}t)}, \quad \text{for } t \gg \tau_m, \tau_{im}, \tag{B 8}$$

with $D_{eff} = D/(1 + \tau_{im}/\tau_m)$.

B.4. Density at short to intermediate time scales

Here, we analyse the regime $t \ll \tau_{im}$. The case $f_m = 1$ and $f_{im} = 0$ is considered in §3. We consider the case $f_{im} = 1$ and $f_m = 0$ here. From $n(x, s)$ (2.3), we obtain, with $s\tau_{im} \gg 1$ and $\phi(s) \sim s + 1/\tau_m$,

$$n_{tot}(x, s) \sim \frac{s\tau_m + 1}{s^2 \tau_{im} \tau_m} \frac{1}{\sqrt{4D(s + 1/\tau_m)}} e^{-\sqrt{(s+1/\tau_m)/D}|x|} + \left(\frac{1}{s} - \frac{1}{s^2\tau_{im}}\right), \quad \text{for } s\tau_{im} \gg 1. \tag{B 9}$$

In the time domain in the limit $t \ll \tau_{im}$, this corresponds to the expression

$$n_{tot}(x, t) \sim \int_0^t \frac{t + \tau_m - t'}{\tau_{im}\tau_m} \exp\left(\frac{-t'}{\tau_m}\right) \frac{\exp\left(-\frac{x^2}{4Dt'}\right)}{\sqrt{4Dt'}} \, dt' + (1 - t/\tau_{im})\delta(x)$$
$$= \frac{e^{-(x^2/4Dt)}}{\sqrt{4\pi D t}} e^{-t/\tau_m} \frac{t}{\tau_{im}} + (1 - t/\tau_{im})\delta(x)$$
$$+ \frac{\exp(-|x|/\sqrt{D\tau_m})}{\sqrt{4D\tau_m}} \left(t/\tau_{im} - |x|\sqrt{\frac{\tau_m}{4D\tau_{im}^2}} + \tau_m/2\tau_{im}\right) \frac{1 - \mathrm{erf}\left(|x|/\sqrt{4Dt} - \sqrt{t/\tau_m}\right)}{2} \tag{B 10}$$

$$- \frac{\exp(|x|/\sqrt{D\tau_m})}{\sqrt{4D\tau_m}} \left(t/\tau_{im} + |x|\sqrt{\frac{\tau_m}{4D\tau_{im}^2}} + \tau_m/2\tau_{im}\right) \frac{1 - \mathrm{erf}\left(|x|/\sqrt{4Dt} + \sqrt{t/\tau_m}\right)}{2}. \tag{B 11}$$

Normalization is preserved, as can be seen by integrating (B 10) over x. The first summand in (B 10) then resolves to t/τ_{im}. In the limit $t \ll \tau_m$, τ_{im}, we recover the short-time behaviour for $n_{tot}(x, t)$ (B 4), as shown in figure 9. For $\tau_m \ll t \ll \tau_{im}$ and $|x| \ll \sqrt{4D\tau_{im}^2/\tau_m}$, we recover the Laplacian intermediate regime in (B 7) with $f_{im} = 1$ and $f_m = 0$. In figure 9, we show a verification of (B 11). For arbitrary fractions of initially mobile tracers, we combine equation (B 11) for immobile initial

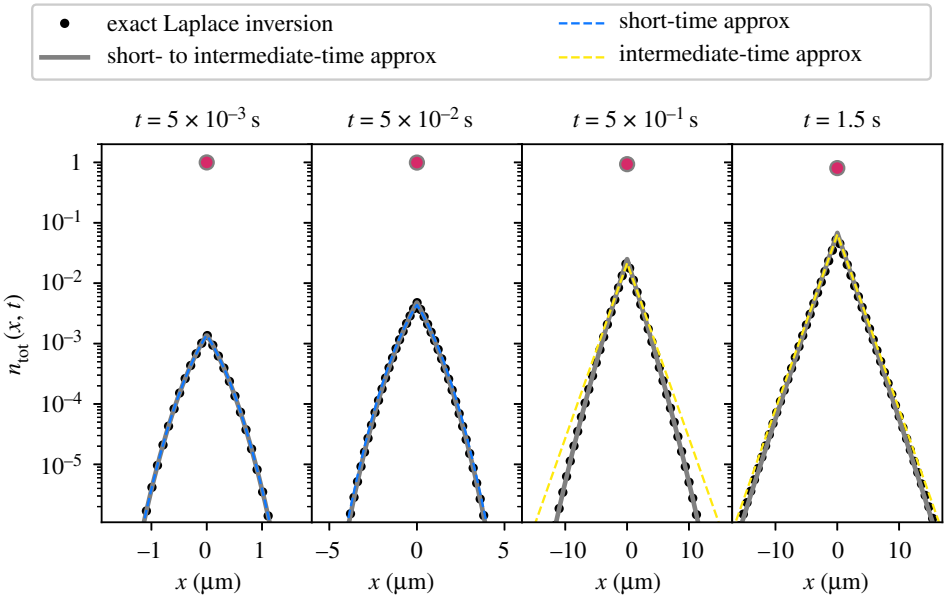

Figure 9. All tracers initially immobile. Comparison of the exact Laplace inversion of (2.3), the short-time approximation (B 4), the intermediate-time approximation (B 7) and the short- to intermediate-time approximation (B 11).

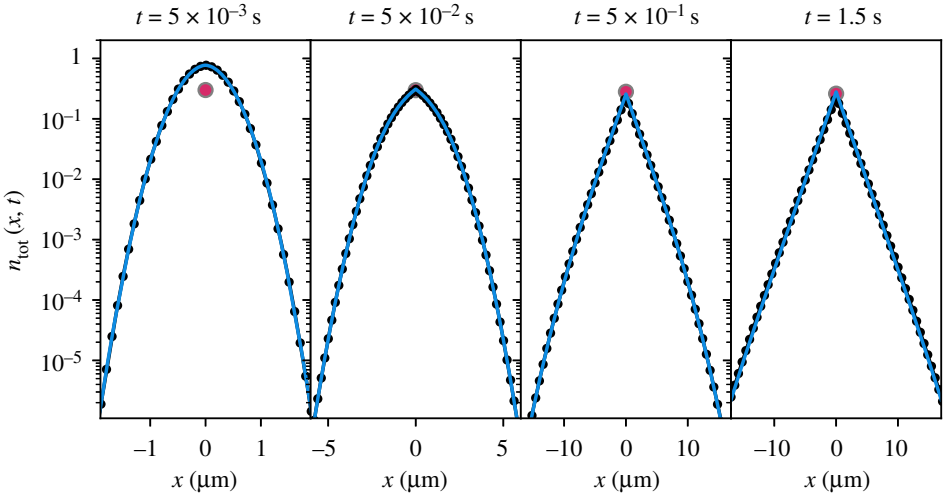

Figure 10. Total concentration $n_{tot}(x, t)$ for $f_{im} = 3/10$ and $f_m = 7/10$. Expression (B 12) is shown as the blue line and the Laplace inversion of $n_{tot}(x, s)$ (2.3) is shown as the black line with markers. Both overlap over five decades in amplitude, for all times shown. The red marker with the grey edge at $x = 0$ denotes the initially immobile tracers that have not yet moved. At short times, the distribution consists of the particles at $x = 0$ and a Gaussian. At $t = 1$ s, the distribution follows a Laplace distribution (linear tails in the log-linear plot), on top of the particles at $x = 0$.

conditions with equation (3.4) for mobile initial conditions, as follows:

$$\begin{aligned} n_{tot}(x, t) \sim{}& \frac{e^{-(x^2/4Dt)}}{\sqrt{4\pi Dt}}\, e^{-t/\tau_m}\left(f_m + f_{im}\frac{t}{\tau_{im}}\right) + f_{im}(1 - t/\tau_{im})\delta(x) \\ &+ \left[f_m + f_{im}\left(t/\tau_{im} - |x|\sqrt{\frac{\tau_m}{4D\tau_{im}^2}} + \tau_m/2\tau_{im}\right)\right] \\ &\times \frac{\exp(-|x|/\sqrt{D\tau_m})}{\sqrt{4D\tau_m}}\,\frac{1 - \mathrm{erf}\left(|x|/\sqrt{4Dt} - \sqrt{t/\tau_m}\right)}{2} \\ &- \left[f_m + f_{im}\left(t/\tau_{im} + |x|\sqrt{\frac{\tau_m}{4D\tau_{im}^2}} + \tau_m/2\tau_{im}\right)\right] \\ &\times \frac{\exp(|x|/\sqrt{D\tau_m})}{\sqrt{4D\tau_m}}\,\frac{1 - \mathrm{erf}\left(|x|/\sqrt{4Dt} + \sqrt{t/\tau_m}\right)}{2}. \end{aligned} \tag{B 12}$$

In figure 10, expression (B 12) is compared with the Laplace inversion of the exact expression of $n_{tot}(x, s)$ (2.3).

References

1. Biggar JW, Nelson DR. 1967 Miscible displacement and leaching phenomena. In *Irrigation of agricultural lands* (ed. RM Hagen), pp. 254–274. Agronomy Monographs, vol. 11. Madison, WI: American Society of Agronomy.
2. Lapidus L, Amundson NR. 1952 Mathematica of adsorption in beds. VI. The effect of longitudinal diffusion in ion exchange and chromatographics columns. *J. Phys. Chem.* **56**, 984–988. (doi:10.1021/j150500a014)
3. Deans HH. 1963 A mathematical model for dispersion in the direction of flow of porous media. *Soc. Pet. Eng. J.* **3**, 49–52. (doi:10.2118/493-PA)
4. Coats KH, Smith BD. 1964 Dead-end pore volume and dispersion in porous media. *Soc. Pet. Eng. J.* **4**, 73–84. (doi:10.2118/647-PA)
5. Van Genuchten MT, Wierenga PJ. 1976 Mass transfer studies in sorbing porous media I. Analytical solutions. *Soil Sci. Soc. Am. J.* **40**, 473–480. (doi:10.2136/sssaj1976.03615995004000040011x)
6. Haggerty R, Gorelick SM. 1995 Multiple-rate mass transfer for modeling diffusion and surface reactions in media with pore-scale heterogeneity. *Water Res. Res.* **31**, 2383–2400. (doi:10.1029/95WR10583)
7. Dentz M, Berkowitz B. 2003 Transport behavior of a passive solute in continuous time random walks and multirate mass transfer. *Water Res. Res.* **39**, 1. (doi:10.1029/2001WR001163)
8. Sardin M, Schweich D, Leij FJ, van Genuchten MT. 1991 Modeling the nonequilibrium transport of linearly interacting solutes in porous media: a review. *Water Res. Res.* **27**, 2287–2307. (doi:10.1029/91WR01034)
9. Schmidlin FW. 1977 Theory of trap-controlled transient photoconduction. *Phys. Rev. B* **16**, 2362–2385. (doi:10.1103/PhysRevB.16.2362)
10. Villermaux J. 1987 A flexible method for representing complex phenomena from simple concepts. *J. Chromatogr.* **406**, 11–26. (doi:10.1016/S0021-9673(00)94014-7)
11. Roth K, Jury WA. 1993 Linear transport models for adsorbing solutes. *Water Res. Res.* **29**, 1195–1203. (doi:10.1029/92WR02537)
12. Metzler R, Klafter J. 2000 The random walk's guide to anomalous diffusion: a fractional dynamics approach. *Phys. Rep.* **339**, 1–77. (doi:10.1016/S0370-1573(00)00070-3)
13. Boggs JM, Young SC, Beard LM, Gelhar LW, Rehfeldt KR, Adams EE. 1992 Field study of dispersion in a heterogeneous aquifer: 1. Overview and site description. *Water Res. Res.* **28**, 3281–3291. (doi:10.1029/92WR01756)
14. Goeppert N, Goldscheider N, Berkowitz B. 2020 Experimental and modeling evidence of kilometer-scale anomalous tracer transport in an alpine karst aquifer. *Water Res.* **178**, 115755. (doi:10.1016/j.watres.2020.115755)
15. Schumer R, Benson DA, Meerschaert MM, Baeumer B. 2003 Fractal mobile/immobile solute transport. *Water Res. Res.* **39**, 13. (doi:10.1029/2003wr002141)
16. Doerries TJ, Chechkin AV, Schumer R, Metzler R. 2022 Rate equations, spatial moments, and concentration profiles for mobile-immobile models with power-law and mixed waiting time distributions. *Phys. Rev. E* **105**, 014105. (doi:10.1103/PhysRevE.105.014105)
17. Igaev M, Janning D, Sündermann F, Niewidok B, Brandt R, Junge W. 2014 A refined reaction-diffusion model of tau-microtubule dynamics and its application in FDAP analysis. *Biophys. J.* **107**, 2567–2578. (doi:10.1016/j.bpj.2014.09.016)
18. Janning D *et al.* 2014 Single-molecule tracking of tau reveals fast kiss-and-hop interaction with microtubules in living neurons. *Mol. Biol. Cell.* **25**, 3541–3551. (doi:10.1091/mbc.e14-06-1099)
19. Yeung C, Shtrahman M, Wu XL. 2007 Stick-and-diffuse and caged diffusion: a comparison of two models of synaptic vesicle dynamics. *Biophys. J.* **92**, 2271–2280. (doi:10.1529/biophysj.106.081794)
20. Sprague BL, Pego RL, Stavreva DA, McNally JG. 2004 Analysis of binding reactions by fluorescence recovery after photobleaching. *Biophys. J.* **86**, 3473–3495. (doi:10.1529/biophysj.103.026765)
21. Liu Z, Legant WR, Chen BC, Li L, Grimm JB, Lavis LD, Betzig E, Tjian R. 2014 3D imaging of Sox2 enhancer clusters in embryonic stem cells. *elife* **3**, e04236. (doi:10.7554/elife.04236)
22. Mazza D, Abernathy A, Golob N, Morisaki T, McNally JG. 2012 A benchmark for chromatin binding measurements in live cells. *Nucleic Acids Res.* **40**, e119. (doi:10.1093/nar/gks701)
23. Chen J *et al.* 2014 Single-molecule dynamics of enhanceosome assembly in embryonic stem cells. *Cell* **156**, 1274–1285. (doi:10.1016/j.cell.2014.01.062)
24. Wu MM, Covington ED, Lewis RS. 2014 Single-molecule analysis of diffusion and trapping of STIM1 and Orai1 at endoplasmic reticulum–plasma membrane junctions. *Mol. Biol. Cell* **25**, 3672–3685. (doi:10.1091/mbc.e14-06-1107)
25. Park S, Lee OC, Durang X, Jeon JH. 2021 A mini-review of the diffusion dynamics of DNA-binding proteins: experiments and models. *J. Korean Phys. Soc.* **78**, 408–426. (doi:10.1007/s40042-021-00060-y)
26. Tafvizi A, Mirny LA, van Oijen AM. 2011 Dancing on DNA: kinetic aspects of search processes on DNA. *ChemPhysChem* **12**, 1418–1489. (doi:10.1002/cphc.201100112)
27. Tafvizi A, Huang F, Fersht AR, Mirny LA, van Oijen AM. 2011 A single-molecule characterization of p53 search on DNA. *Proc. Natl Acad. Sci. USA* **108**, 563–568. (doi:10.1073/pnas.1016020107)
28. Kong M *et al.* 2016 Single-molecule imaging reveals that Rad4 employs a dynamic DNA damage recognition process. *Mol. Cell* **64**, 376–387. (doi:10.1016/j.molcel.2016.09.005)
29. Kamagata K, Mano E, Ouchi K, Kanabayashi S, Johnson RC. 2018 High free-energy barrier of 1D diffusion along DNA by architectural DNA-binding proteins. *J. Mol. Biol.* **430**, 655–667. (doi:10.1016/j.jmb.2018.01.001)
30. Kolarova M, García-Sierra F, Bartos A, Ricny J, Ripova D. 2012 Structure and pathology of tau protein in Alzheimer disease. *J. Alzheimer's Dis.* **2012**, 731526. (doi:10.1155/2012/731526)
31. Guo T, Noble W, Hanger DP. 2017 Roles of tau protein in health and disease. *Acta Neuropathol.* **133**, 665–704. (doi:10.1007/s00401-017-1707-9)
32. Mora S, Pomeau Y. 2018 Brownian diffusion in a dilute field of traps is Fickean but non-Gaussian. *Phys. Rev. E* **98**, 040101. (doi:10.1103/PhysRevE.98.040101)
33. Wang B, Anthony SM, Bae SC, Granick S. 2009 Anomalous yet Brownian. *Proc. Natl Acad. Sci. USA* **106**, 15160–15164. (doi:10.1073/pnas.0903554106)
34. Skaug MJ, Mabry J, Schwartz DK. 2013 Intermittent molecular hopping at the solid-liquid interface. *Phys. Rev. Lett.* **110**, 256101. (doi:10.1103/PhysRevLett.110.256101)
35. Chakraborty I, Roichman Y. 2020 Disorder-induced Fickian, yet non-Gaussian diffusion in heterogeneous media. *Phys. Rev. Res.* **2**, 022020. (doi:10.1103/PhysRevResearch.2.022020)
36. Chechkin AV, Seno F, Metzler R, Sokolov IM. 2017 Brownian yet non-Gaussian diffusion: from superstatistics to subordination of diffusing diffusivities. *Phys. Rev. X* **7**, 021002. (doi:10.1103/physrevx.7.021002)
37. Chubynsky MV, Slater GW. 2014 Diffusing diffusivity: a model for anomalous, yet Brownian, diffusion. *Phys. Rev. Lett.* **113**, 098302. (doi:10.1103/PhysRevLett.113.098302)
38. Wang B, Kuo J, Bae SC, Granick S. 2012 When Brownian diffusion is not Gaussian. *Nat. Mater.* **11**, 481–485. (doi:10.1038/nmat3308)
39. Sposini V, Chechkin AV, Seno F, Pagnini G, Metzler R. 2018 Random diffusivity from stochastic equations: comparison of two models for Brownian yet non-Gaussian diffusion. *New J. Phys.* **20**, 043044. (doi:10.1088/1367-2630/aab696)
40. Lanoiselée Y, Grebenkov DS. 2018 A model of non-Gaussian diffusion in heterogeneous media. *J. Phys. A: Math. Theor.* **51**, 145602. (doi:10.1088/1751-8121/aab15f)
41. Jain R, Sebastian KL. 2016 Diffusion in a crowded, rearranging environment. *J. Phys. Chem. B* **120**, 3988–3992. (doi:10.1021/acs.jpcb.6b01527)
42. Javanainen M, Hammaren H, Monticelli L, Jeon JH, Metzler R, Vattulainen I. 2013 Anomalous and normal diffusion of proteins and lipids in crowded lipid membranes. *Faraday Discuss.* **161**, 397–417. (doi:10.1039/C2FD20085F)
43. Yamamoto E, Akimoto T, Mitsutake A, Metzler R. 2021 Universal relation between instantaneous diffusivity and radius of gyration of proteins in

aqueous solution. *Phys. Rev. Lett.* **126**, 128101. (doi:10.1103/PhysRevLett.126.128101)

44. Baldovin F, Orlandini E, Seno F. 2019 Polymerization induces non-Gaussian diffusion. *Front. Phys.* **7**, 124. (doi:10.3389/fphy.2019.00124)
45. Hidalgo-Soria M, Barkai E. 2020 The hitchhiker model for Laplace diffusion processes in the cell environment. *Phys. Rev. E* **102**, 012109. (doi:10.1103/PhysRevE.102.012109)
46. Skinner TOE, Schnyder SK, Aarts DGAL, Horbach J, Dullens RPA. 2013 Localization dynamics of fluids in random confinement. *Phys. Rev. Lett.* **111**, 128301. (doi:10.1103/PhysRevLett.111.128301)
47. Wang D, Wu H, Liu L, Chen J, Schwartz DK. 2019 Diffusive escape of a nanoparticle from a porous cavity. *Phys. Rev. Lett.* **123**, 118002. (doi:10.1103/PhysRevLett.123.118002)
48. Ślęzak J, Burov S. 2021 From diffusion in compartmentalized media to non-Gaussian random walks. *Sci. Rep.* **11**, 1. (doi:10.1038/s41598-020-79139-8)
49. Miotto JM, Pigolotti S, Chechkin AV, Roldán-Vargas S. 2021 Length scales in Brownian yet non-Gaussian dynamics. *Phys. Rev. X* **11**, 031002. (doi:10.1103/PhysRevX.11.031002)
50. Peterson EM, Manhart MW, Harris JM. 2016 Single-molecule fluorescence imaging of interfacial DNA hybridization kinetics at selective capture surfaces. *Anal. Chem.* **88**, 1345–1354. (doi:10.1021/acs.analchem.5b03832)
51. Scholz T, Mandelkow E. 2014 Transport and diffusion of Tau protein in neurons. *Cell. Mol. Life Sci.* **71**, 3139–3150. (doi:10.1007/s00018-014-1610-7)
52. Mercken M, Fischer I, Kosik KS, Nixon RA. 1995 Three distinct axonal transport rates for tau, tubulin, and other microtubule-associated proteins: evidence for dynamic interactions of tau with microtubules in vivo. *J. Neurosci.* **15**, 8259–8267. (doi:10.1523/JNEUROSCI.15-12-08259.1995)
53. Kreis TE, Birchmeier W. 1982 Microinjection of fluorescently labeled proteins into living cells with emphasis on cytoskeletal proteins. *Int. Rev. Cytol.* **75**, 209–227. (doi:10.1016/s0074-7696(08)61005-0)
54. Ghosh SK, Cherstvy AG, Metzler R. 2015 Non-universal tracer diffusion in crowded media of non-inert obstacles. *Phys. Chem. Chem. Phys.* **17**, 1857–1858. (doi:10.1039/c4cp03599b)
55. Javanainen M, Hammaren H, Monticelli L, Jeon J-H, Miettinen MS, Martinez-Seara H, Metzler R, Vattulainen I. 2013 Anomalous and normal diffusion of proteins and lipids in crowded lipid membranes. *Faraday Discuss.* **161**, 397–417. (doi:10.1039/C2FD20085F)
56. Miyaguchi T, Akimoto T, Yamamoto E. 2016 Langevin equation with fluctuating diffusivity: a two-state model. *Phys. Rev. E* **94**, 012109. (doi:10.1103/PhysRevE.94.012109)
57. Hidalgo-Soria M, Barkai E, Burov S. 2020 Cusp of non-Gaussian density of particles for a diffusing diffusivity model. *Entropy* **23**, 231. (doi:10.3390/e23020231)
58. Vitaly S, Paradisi P, Pagnini G. 2022 Anomalous diffusion originated by two Markovian hopping-trap mechanisms. *J. Phys. A: Math. Theor.* **55**, 224012. (doi:10.1088/1751-8121/ac677f)